Case Studies in Construction Materials 17 (2022) e01538

Contents lists available at ScienceDirect

Case Studies in Construction Materials

journal homepage: www.elsevier.com/locate/cscm

Load carrying behavior of concrete reinforced with bundled BFRP bars by using DIC

Bruno Ribeiro [a,*], Hisafumi Asaue [a], Atsushi Hattori [a], Tomoki Shiotani [a], Takumi Kobayashi [b], Junya Sato [b], Masakazu Uchida [b], Masahiro Ishida [b]

[a] Kyoto University, Graduate School of Engineering, Japan
[b] Public Works Research Institute, Center for Advanced Engineering Structural Assessment and Research, Japan

ARTICLE INFO

Keywords:
Basalt fiber-reinforced polymer
Bundled bars
Load carrying behavior
Load-deflection relationship
Digital image correlation

ABSTRACT

Recently, basalt fiber-reinforced polymer (BFRP) has gained attention in the construction industry because of its worldwide availability and eco-friendly nature. Different from conventional steel bars, BFRP bar do not corrode being an ideal reinforcing material in structures surrounding magnetic fields and marine environments, given its chemical stability. This study investigated the load carrying behavior of concrete beams reinforced with conventional deformed steel bars and seven-bundled BFRP bars through four-point flexural test. For each case, two beams were prepared; one beam was designed with a low reinforcement ratio and another with a high reinforcement ratio in order to obtain a load carrying capacity of around 330–368 kN and 483–519 kN, respectively. Deflection, crack width evolution, and strain behavior of each beam were comparatively analyzed using a digital image correlation (DIC) based technique. The DIC analysis results showed that the neutral axis of bundled BFRP reinforced cases move to the upper end in an early loading stage, with larger cracks width, and the deflection is larger in BFRP cases than in those of steel-reinforced beams with the respective reinforcement ratio. However, the four-point flexural test results revealed that bundled BFRP bars can be used as an alternative to conventional steel bars. The load carrying capacities were obtained similarly to designed values, around 364 and 551 kN for low and high reinforcement ratio cases, respectively.

1. Introduction

Concrete has been used for a long time because it is considered a cheap material, accessible, easy to handle, durable, and highly resistant against compression. However, concrete has its disadvantage: it is a brittle material due to its low resistance against tensile stress. In order to improve the tensile resistance, steel bars are used to reinforce the concrete.

Steel reinforced concrete is widely used throughout the world. However, the major deterioration of infrastructures is linked to steel corrosion in concrete [1–4]. The corrosion of the steel reinforcement results in durability reduction of the whole structure [4] in which repairs should be applied. Consequently, it raises costs in the life cycle of the structure [5]. The corrosion of the steel in concrete may be for several factors. The two most important factors are the penetration of chlorides [6–9] by the concrete surface and the absorption of CO_2 into the concrete [10–12]. Both factors are linked to the break of the passive film of the steel surface. With the break of the passive film, the corrosion tends to be faster, and due to the formation of corrosion products on the steel surface, it leads to the development of

* Corresponding author.
E-mail address: brunoribeiro2006@hotmail.com (B. Ribeiro).

https://doi.org/10.1016/j.cscm.2022.e01538
Received 1 August 2022; Received in revised form 28 September 2022; Accepted 4 October 2022
Available online 12 October 2022

cracks on the concrete cover. It easily allows the penetration of other deterioration factors, such as water, oxygen, and chemicals, into the concrete, accelerating steel corrosion. Although steel-reinforced concrete structures are economically feasible, costs with inspections, maintenance, repairs, and monitoring systems tend to increase the cost of the structure. Furthermore, some countries are expected to suffer from a lack of workforce. In countries where the population is elderly, for instance, in Japan, labor for the inspections, maintenance, and repairs has a propensity to suffer in the near future. Accordingly, the lack of inspections may make structures more prone to collapse.

Various studies have been done in order to find a new replacement for steel bars used in concrete structures in harsh environments. Epoxy-coated steel rebar and galvanized steel rebar are some examples of countermeasures used in structures in harsh environments [13–15]. However, the corrosion is expected to start later than the conventional steel bar, but it cannot wholly prevent corrosion. Recently, many researchers have seen the fiber-reinforced polymer (FRP) as a possible material to replace conventional steel bars [3, 16–19]. This is because FRP bars offer many advantages such as corrosive resistance, high strength-to-weight ratio, ease of handling, and non-magnetic properties [16,20,21].

Many previous studies about FRP reinforced concrete can be found in the literature [16,22–26]. Durability performance of FRP reinforcing bars, flexural capacity, crack spacing and width, and difference in failure modes of FRP reinforced concrete beams are some examples of investigations that have been done. Furthermore, some studies have considered the deflection behavior of FRP reinforced concrete. The low modulus of elasticity and the linear stress-strain diagram (with respect to steel) are examples that FRP reinforcement faces against its application in concrete structures since it affects the serviceability of the concrete members [16]. Grace et al. [27] presented experimental results of seven simple rectangular beams reinforced with bars and stirrups made of steel, carbon, and glass fiber reinforced polymer. The study concluded that FRP arrangements have the same load capacity as conventional steel-reinforced beams, although the ductility and the failure mode differed [27].

As can be seen, there are different types of FRP. Besides carbon-, aramid-, and glass-reinforced polymers, basalt-reinforced polymers are also used [1,16,28–31]. Basalt-reinforced polymer (BFRP) is composed of basalt fibers fabricated from basalt rock and polymer resins, such as epoxy or vinyl ester. Besides basalt rock being an inorganic material and worldwide, basalt fibers are referred to as an eco-friend material [32,33]. For this reason, they have been attracting the attention of the construction industry [34]. Therefore, due to the lack of experimental data on bundled FRP in the literature, the necessity for further research [19,35], and concerns about cracking properties and shear deformation of concrete beams reinforced with BFRP bars, this paper aims to clarify the load carrying behavior of concrete beams reinforced with bundled BFRP bars. Bundling bars may be useful within the lack of larger diameter bars and can be ensured, in a pseudo manner, the load carrying capacity. Applying different materials with different arrangements is important to offer unique design options resulting in a widespread application of new materials. Four beams were prepared, two for each type of reinforcement. Two specimens were designed with a low reinforcement ratio, and another two were projected with a high reinforcement ratio. The comparison among the cases was made from flexural strength, strains, deflection, cracks width, and spacing differences.

2. Experimental program

2.1. Materials

Table 1 shows the mix proportion of concrete used to prepare the specimens. As shown in Table 1, all beams were made using ready-mixed concrete Normal/36/12/20/N, conforming to JIS A 5308 [36]. Ordinary Portland cement (C, density: 3.15 g/cm^3) was used, and the water to cement ratio (W/C) was 44%. Two types of fine aggregates (S1, density: 2.58 g/cm^3 and S2, density: 2.65 g/cm^3) and a coarse aggregate (G, density: 2.66 g/cm^3) with a nominal maximum size (NMS) of 20 mm were used. The fine aggregate ratio was 46.1%. A market available air-entraining agent (AEA) was also used in order to increase the workability of the concrete.

In addition, 12 specimens (φ100 × 200 mm) were cast in order to determine the average compressive strength (JIS A 1108) [37] and elasticity modulus (JIS A 1149) [38]. As shown in Table 1, the slump (JIS A 1101) [39], compressive strength, and elastic modulus of the concrete were 12 cm, 45.1 N/mm^2, and 32.57 kN/mm^2, respectively.

Fig. 1 shows the longitudinal reinforcements and Table 2 lists the properties of the reinforcing bars and total mass in each case. Regarding the material properties shown in Table 2, it was obtained from experimental tests for BFRP reinforcements, while in the case of steel reinforcement, it was provided by the manufacturer.

As shown in Fig. 1, the BFRP bars used in this research were made of basalt fiber impregnated with polypropylene. The diameter of a single BFRP bar is 4.45 mm, and seven single bars were bundled, forming a seven-bundled BFRP with a nominal diameter of 13.35 mm. Fig. 1 also shows the steel deformed bars used in this research, in conforming to JIS G 3112 [40].

As shown in Table 2, the BFRP bars have a cross-sectional area of 79.4 mm^2. The cross-sectional area was calculated using only the effective diameter of the basalt fiber cross-section. For all cases, deformed steel bars with a diameter of 9.53 mm were used to make the stirrups used in this research. Further details of each beam case are provided in the following section.

Table 1
Mix proportion, fresh and hardened properties of the concrete.

W/C	s/a	NMS	Unit mass (kg/m^3)						Slump	Compressive Strength	Modulus of elasticity
(%)	(%)	(mm)	C	W	S1	S2	G	AEA	(cm)	(N/mm^2)	(kN/mm^2)
44	46	20	389	171	552	241	947	3.50	12	45.1	32.6

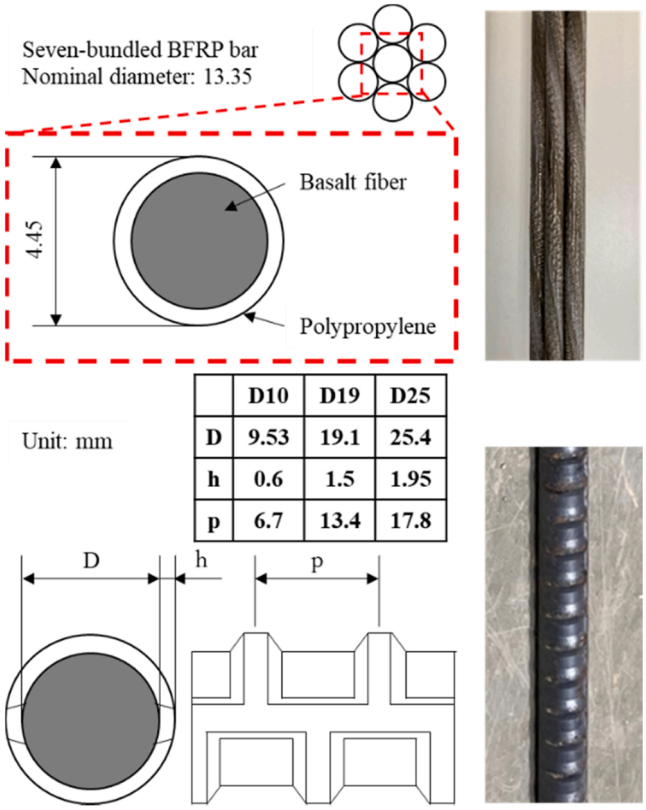

Fig. 1. Reinforcement types used in this research.

Table 2
Properties of the reinforcing bars and total mass in each case.

Case	Reinforcement type	Bar grade*	Nominal diameter (mm)	Cross-sectional area (mm^2)	Tensile strength** (N/mm^2)	Modulus of elasticity (kN/mm^2)	Number of bar	Bar length (mm)	Unit mass (kg/m)	Total mass (kg)
1	Longitudinal BFRP	–	φ13.3	79.4	923	39.3	9	2800	0.159	4.01
	Steel stirrups 1	SD345	D10	71.3	385	200	26	1200	0.560	17.47
2	Longitudinal steel	SD345	D19	286.5	405	200	6	2800	2.250	37.80
	Steel stirrups 1	SD345	D10	71.3	385	200	26	1200	0.560	17.47
3	Longitudinal BFRP	–	φ13.3	79.4	923	39.3	21	2800	0.159	9.35
	Steel stirrups 1	SD345	D10	71.3	385	200	26	1190	0.560	17.33
	Steel stirrups 2	SD345	D10	71.3	385	200	4	340	0.560	0.76
4	Longitudinal steel	SD345	D25	506.7	409	200	6	2800	3.980	66.86
	Steel stirrups 1	SD345	D10	71.3	385	200	26	1210	0.560	17.62

* SD: steel deformed;
** yield strength for steel bar and ultimate strength for seven-blunded BFRP bar

2.2. Beam specimens

Fig. 2 and Table 3 show the details of the beam specimens. The beams were designed according to reference [41]. A total of four reinforced concrete beams were cast and tested. Two beams were reinforced with BFRP bars, and two beams were reinforced with steel bars as reference. The beams were 2900 mm long with a rectangular cross-section of 250 mm in width and 400 mm in depth. Note that the reinforcement bars have been positioned so that their centroids are centered at the predetermined intersection of the lines, as shown in Fig. 2. In addition, all longitudinal reinforcements were not hooked in this research. The reinforcement ratio (ρ) in Table 3 was obtained by dividing the area of steel (As) by the effective area of the cross-section (bd, where b is the breadth and d is the depth).

As shown in Table 3, two beams, one reinforced with BFRP bars (case 1) and another reinforced with steel bars (case 2), were designed with a low reinforcement ratio of 0.71% and 1.71% in order to have a similar load-carrying capacity of approximately 368

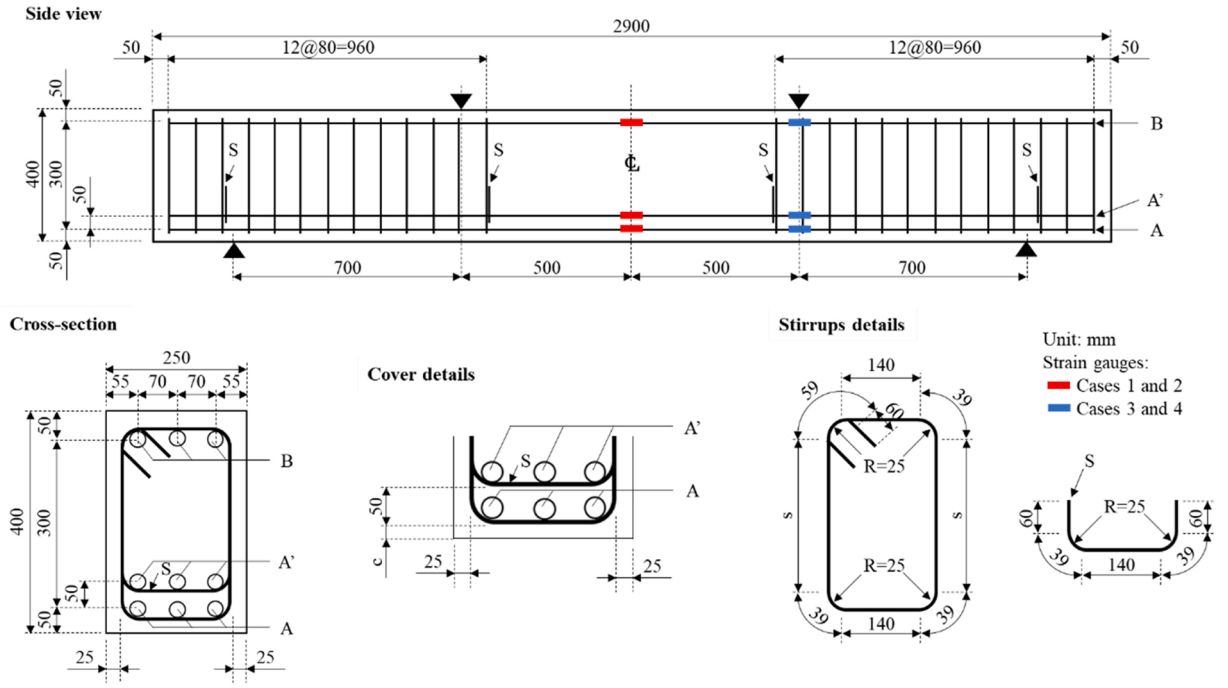

Fig. 2. Dimensions of test beam specimens.

Table 3
Details of reinforcements and their arrangement.

Case	Reinforcement									Stirrups							Cover
	A		Amount	A'		Amount	B		Amount	Ratio (%)	Standard		Amount	s (mm)	S		Amount	c (mm)
1	BFRP φ13.3×2		3	—	—	—	BFRP φ13.3		3	0.71	SD345 D10		26	280	—	—	—	26.7
2	SD345 D19		3	—	—	—	SD345 D19		3	1.71			26	279	—	—	—	30.5
3	BFRP φ13.3×3		3	BFRP φ13.3×3		3	BFRP φ13.3		3	1.66			26	277	SD345 D10		4	29.5
4	SD345 D25		3	—	—	—	SD345 D25		3	3.04			26	285	—	—	—	27.5

and 330 kN, respectively. On the other hand, the other two beams, one reinforced with BFRP bars (case 3) and another reinforced with steel bars (case 4), were projected with a high reinforcement ratio, 1.66% and 3.04% and a load-carrying capacity of approximately 519 and 483 kN, respectively. However, it should be noted that to achieve similar load-carrying capacity requirements, the arrangement of the bars is different in cases 3 and 4.

Fig. 3. Four-point flexural test setup.

2.3. Test setup and instrumentation

As demonstrated in Fig. 3, the flexural test [42] was carried out by a 700 kN hydraulic actuator bolted to an independent loading frame was used to apply monotonic concentrated loading on the midpoint of a rigid steel spreader beam. This spreader beam was used to deliver two equal concentrated loads to the midpoint of each span. Note that one load cell was used to measure the reaction at the midpoint of the spreader beam.

2.4. Digital image correlation

Digital image correlation (DIC) is a non-contact and optical measurement method adopted to track the displacements on a surface of an object, such as concrete [3,43–46]. The images before, during, and after the deformation of an interested surface are taken by two digital cameras. The deformation, displacement, and strain at any point of the image can be computed from those images. Compared to conventional measurement methods, such as strain gauges and linear variable differential transformers (LVDTs), DIC is relatively cheap, and its measurement's precision is high. Another advantage is that DIC can provide an entire field measurement which allows seeing the stress location during and after the testing.

In both, steel and BFRP beams specimens, the digital images were acquired constantly as the specimens were loaded. The digital cameras have a resolution of 3376 × 2704 pixels. The cameras were set up approximately 2 m from the specimen in order to obtain an image of the area of interest (AOI) within approximately 1000 and 450 mm. In cases 1 and 2, the center of the AOI was set at the midpoint of the specimen. In cases 3 and 4, the center of the AOI was set at 500 mm left from the midpoint of the specimen.

As shown in Fig. 5, the speckle pattern was made on the specimen. First, the AOI was spray-painted onto each beam in white color. Right after, an irregular pattern of black dots was prepared over it, using black spray paint. The images of the interface specimen are captured before loading and during various stages of loading. The images were captured automatically to avoid any vibration and keep the distance between the camera lens and the specimen unchanged. The digital images taken during the experiments for steel and BFRP specimens are correlated using the software Vic-3D 7.

In addition, seven LVDTs were used to measure the deflection in different locations. As shown in Fig. 4, the LVDTs were set at the midpoint and 500, 850, and 1200 mm from the midpoint in both directions. The beams were continuously supported over two equal clear spans of 1200 mm each.

3. Results and discussions

3.1. Load-deflection relationship

Fig. 6 illustrates the relationship between load and mid-span deflection during the flexural test. As shown in Fig. 6, the load carrying capacities of bundled BFRP bar reinforced beams were obtained similarly to designed values, around 364 and 551 kN for low and high reinforcement ratio cases, respectively. In addition, at the early stage of the test, all BFRP and steel reinforced concrete beams present a similar stiffness, and the deflection of the beams was minimal until the development of the first crack. However, after the appearance of the first crack, the stiffness of both cases changes. While the stiffness of steel reinforced concrete beams decreases slightly, the stiffness of BFRP beams decreases considerably. In addition, BFRP reinforced concrete beams do not present a yield point as in the case of steel. In the cases of BFRP beams, it is possible to observe that after the first crack, the stiffness of the specimen is similar until the ultimate state. This behavior also could be seen in references [47–50] since it is expected due to the low elastic modulus of FRP bars. Nevertheless, by increasing the reinforcement ratio and placing the longitudinal bars reinforcement in two layers at the lower part of the beam, it was possible to increase the stiffness of the beam and, consequently, increase the load-carrying capacity and decrease the deflection, as shown in case 3. Elgabbas et al. [51] reinforced six beams measuring 3100 × 200 × 300 mm with 8, 12, and 16 mm BFRP bars and under four-point flexural over a clear span of 2700 mm until failure. The authors noticed that the reinforcement ratio significantly influences the post-cracking behavior until failure, where larger deformations were observed for lower reinforcement ratios. Thus, bundled BFRP bar reinforced beams can obtain a similar behavior to those reinforced with single BFRP bars as long as they are reinforced with the same reinforcement ratio.

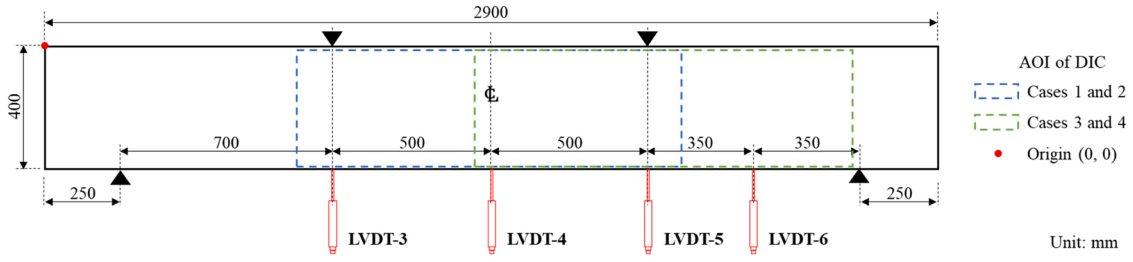

Fig. 4. LVDTs locations and area of interest of DIC.

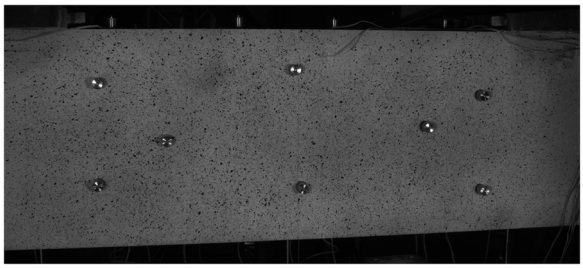

Fig. 5. Speckle pattern made on the specimen surface.

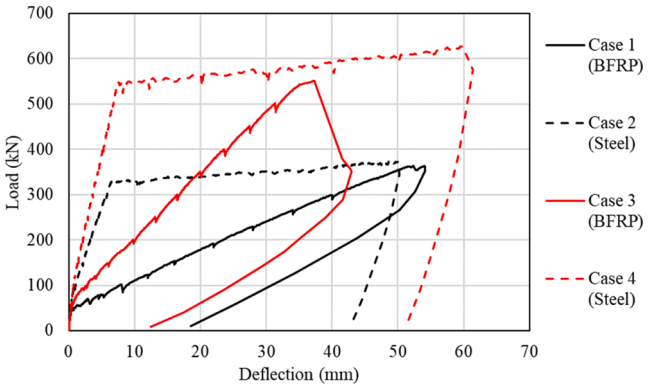

Fig. 6. Load-deflection relationship of specimens.

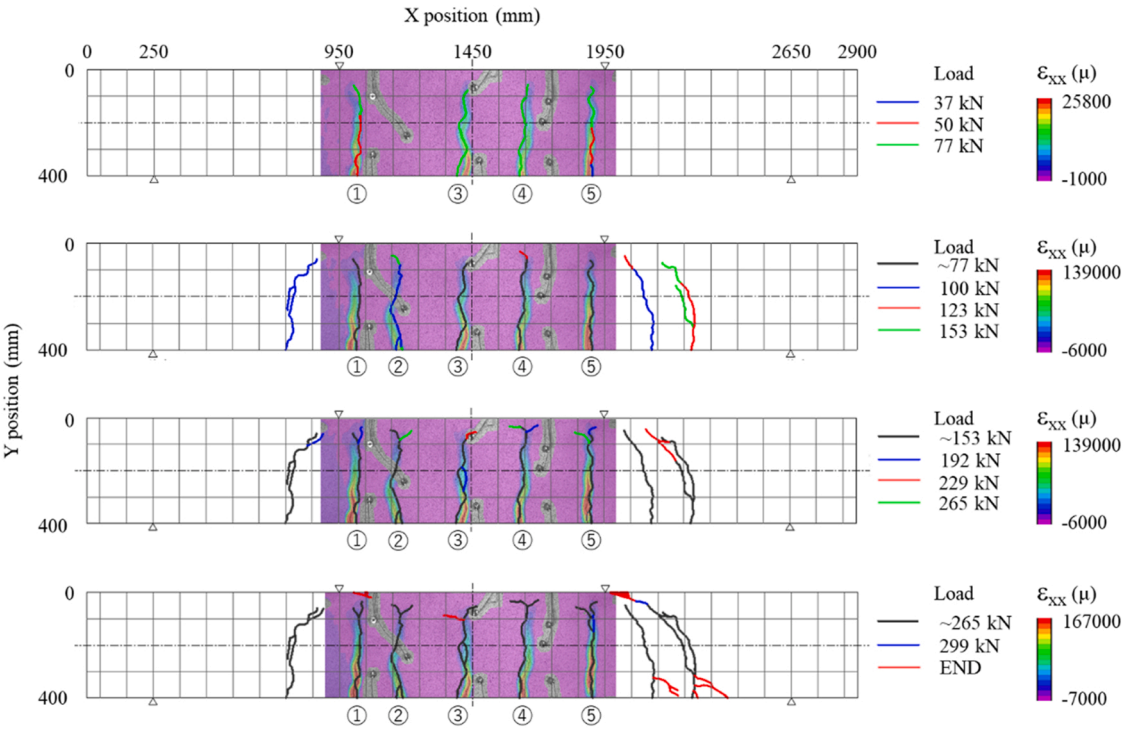

Fig. 7. Crack pattern and strain localization of case 1 (BFRP).

3.2. Crack pattern and width evolution

Fig. 7, Fig. 8, Fig. 9, and Fig. 10 show the crack pattern under different loads and strain localization (ε_{xx}: normal strain on the cross-section directed to the X axis) for cases 1, 2, 3, and 4, respectively. The numbers in the circles correspond to the name of the cracks monitored in this study.

As can be seen in Figs. 7, 8, 9, and 10, the cracks in BFRP beams rise from the bottom towards the top earlier than the cases of steel beams. In case 1, cracks reach a Y position of around 50 mm when the load is 77 kN, while in case 2, the same Y position was reached only before the end of the test, under a load of 322 kN. This same behavior was also observed in cases 3 and 4, where the reinforcement ratio was higher than in cases 1 and 2. The low modulus of elasticity of BFRP reinforcements may be influenced the cracking behavior.

Duic et al. [1] reported that beams reinforced with BFRP bars developed a higher number of flexural tensile cracks than their steel counterparts, probably due to the low stiffness of BFRP bar. However, the beams reinforced with steel in this study showed more distributed cracks, while in BFRP cases, it exhibited a smaller number of cracks which increased the spacing among them. This may be due to the difference in the surface profile of the reinforcements. The steel reinforcement used in this study has a deformed surface differently from BFRP reinforcement which has no surface treatment (smooth surface).

Fig. 11 shows the cumulative width cracks in the steel and BFRP reinforced concrete beams under different loads during the flexural loading test. The detection of the cracks by using DIC is based on longitudinal displacement distribution at the bottom of specimens. The discontinuity signifies the presence of a crack at a certain position within the AOI. The vertical amplitude of each discontinuity indicates the crack width. More details about the measurement steps can be found in reference [52].

As demonstrated in Fig. 11, the first crack appears under a load of 35 and 37 kN for cases 1 and 2 and 45 and 79 kN for cases 3 and 4, respectively. Although some cracks were not observed visually (Figs. 7, 8, 9, and 10), from Fig. 11, it is possible to see a similar number of cracks in this early stage within the bending span of cases 1 and 2, and within the bending span ($\leq$1950 mm) of cases 3 and 4. As shown in Fig. 6, the stiffness of the BFRP cases is smaller than the steel cases. For this reason, the deflection in the BFRP cases is higher, resulting in the development of cracks at an early stage compared to the steel cases.

When the load reaches 100 kN, the number of cracks increases in cases 3 and 4. In both cases, cracks (No. 10 in case 3 and No. 8 in case 4) were developed within the shear span, where the crack No. 10 is 3 times wider than crack No. 8. Furthermore, the vertical amplitude of each discontinuity tends to increase in the BFRP case. As shown in Fig. 11 (case 3), the crack width of cracks number 1 and 5 growths from 0.01 and 0.03 mm to 0.33 and 0.30 mm, respectively. At the same load of 100 kN, in case 4, the width of the cracks is 0.01, 0.04, 0.04, and 0.02 mm for cracks number 1, 3, 6, and 8, respectively.

From Figs. 7, 8, 9, 10, and 11, it is possible to see that by increasing the longitudinal reinforcement ratio, the number of cracks increased, resulting in a reduction in the width of the cracks. Although the results are in agreement with those reported by Elgabbas et al. [51], which used ribbed BFRP bars to reinforce concrete beams, the reduction of crack width probably will be more expected when the surface of the BFRP bars is treated. Even though there is no concern about corrosion in the case of BFRP reinforcements, when cracks are concentrated, and the width becomes large, other concerns arise, such as reinforcement damage, structure aesthetic purposes, and the sense of safety by users. For this reason, it is necessary to consider a BFRP reinforcement that has its surface treated, such as sand coating, fiber winding, indentation, and stranded wire, in order to improve the bond between concrete and BFRP reinforcements [53,54].

In addition, Figs. 7, 8, 9, 10, and Fig. 11 show that it is possible to detect possible cracks' development locations even before the cracks could visually appear. After cracks appear, it is possible to monitor and quantifies the cracks during the whole test by using DIC.

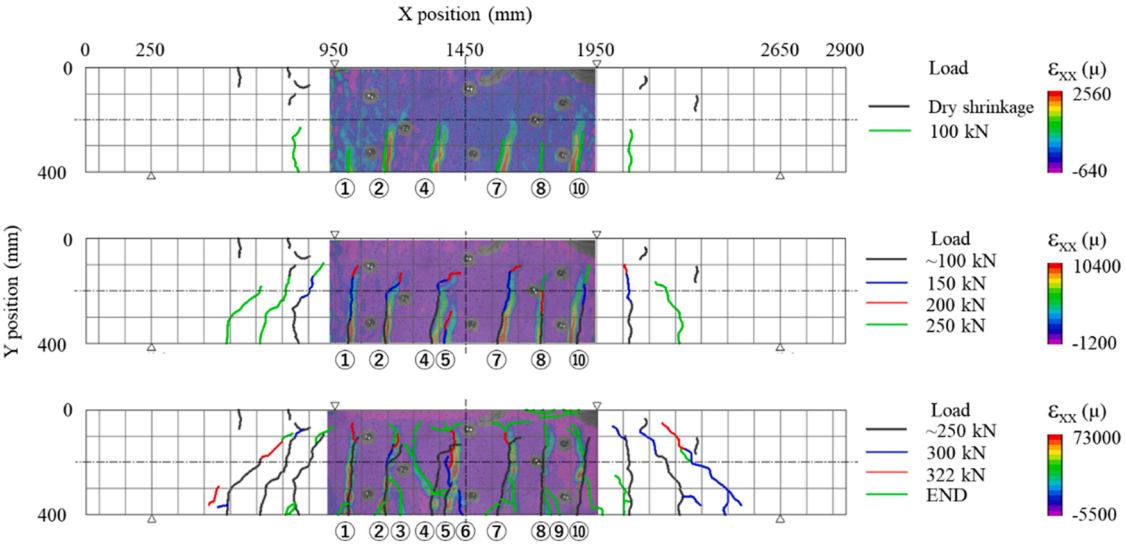

Fig. 8. Crack pattern and strain localization of case 2 (Steel).

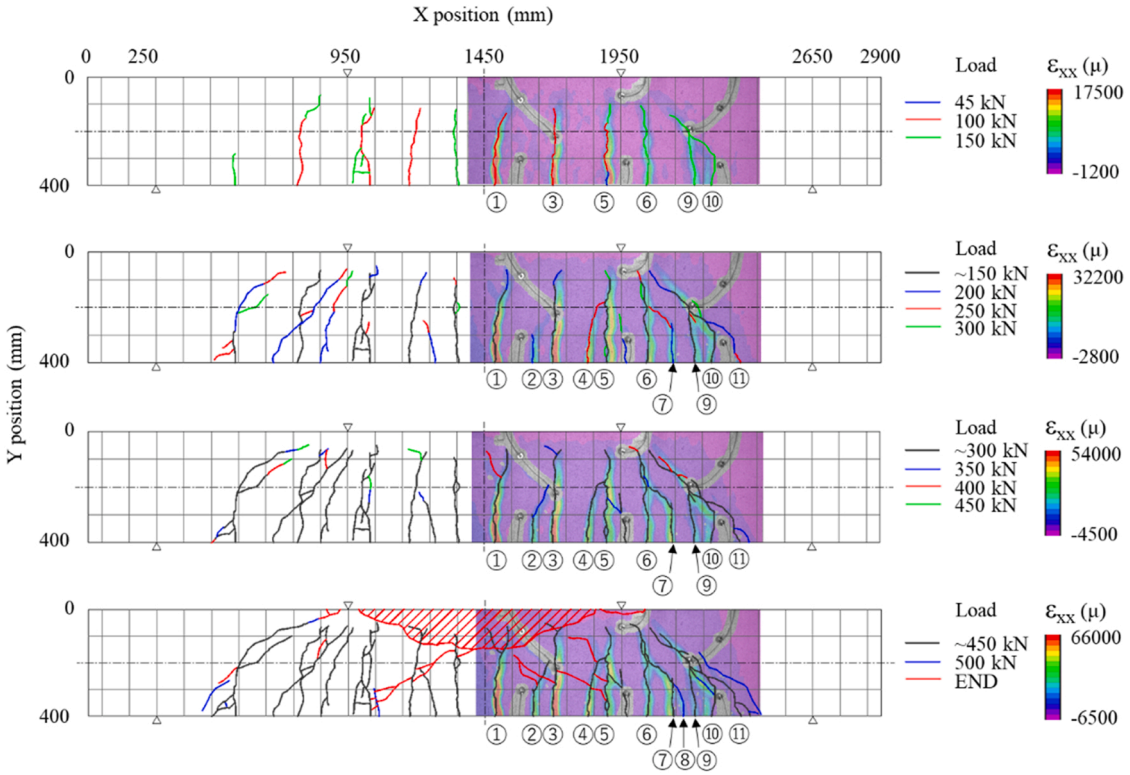

Fig. 9. Crack pattern and strain localization of case 3 (BFRP).

3.3. *Deflection of beams*

Fig. 12 shows the deflection results of steel and BFRP reinforced concrete beams. These results were obtained by LVDTs and DIC through three points of the beams at the bottom surface and at the bottom of the side surface, respectively. It is possible to see from Fig. 12 that the deflection value obtained from DIC and LVDTs are similar, both in steel reinforced concrete beam cases as BFRP reinforced concrete beam cases, from the start of the load until the end of the test.

Fig. 13 shows the deflection of the steel and BFRP reinforced concrete beams at the bottom of the side surface under different loads. Note that these results were obtained by DIC only, which is able to measure the deflection of the AOI continuously. It is possible to see in Fig. 13 that as the specimen is loaded, the larger the deflection.

From Fig. 13 (cases 1 and 2), it is possible to see that the deflection at the bending span is practically symmetrical. After the appearance of the first crack at around 35–50 kN and the decrease of the stiffness, the deflection at the center of the BFRP beam increased from 0.65 to 4.46 mm at 77 kN. This deflection is equivalent to the deflection of the yield point of the steel beam case. Furthermore, the deflection at approximately 300 kN is around eight times more in the BFRP reinforced beam (case 1) than in case 2. As mentioned above, due to the low elastic modulus of BFRP bars, BFRP beams exhibit larger deflections than steel. In addition, the BFRP bar used in this study has a smooth surface (without any surface treatment). A previous study observed that the load-deflection performance of smooth surface BFRP bar reinforced concrete beam was poorest among those that had its surface treated (wrapped, ribbed, and grain-covered) [55]. For this reason, the deflection in the BFRP case in this research was more influenced as the load increase in comparison to the steel case, which was reinforced with deformed steel bars.

As indicated in Fig. 13 (cases 3 and 4), the deflection at the center in the case of BFRP and steel reinforced concrete beam is similar until 45–80 kN, when the first crack is developed. When the load reaches 300 kN, the deflection of the steel reinforced beam is around 3.31 mm, while in the case of the BFRP reinforced concrete beam, the deflection value increase to approximately 16.5 mm. These values are around 39% and 59% smaller than cases 1 and 2, which correspond to 5.47 and 40.2 mm, respectively. As mentioned before, the cross-sectional area of the longitudinal bar in cases 3 and 4 is larger than in cases 1 and 2, which increases the stiffness of the beam avoiding high deflection.

Moreover, as demonstrated in Fig. 13 (cases 3 and 4), when the load of 300 kN is reached in the case of BFRP, the deflection slope is changed near the position of 2150 mm (equivalent to crack number 7). This change may be due to the decrease in the shear transfer capacity, such as aggregate interlocking and dowel action. In order to analyze the load transfer behavior, the slope of deflection was calculated. The results are demonstrated in Fig. 14.

As shown in Fig. 14, the deflection slope of the beams reinforced with BFRP is different from steel case beams. Since the deflection is higher in BFRP beams, the slope in BFRP cases is higher than in steel cases. It is also notable in Fig. 14 that the slope is loose in the cases

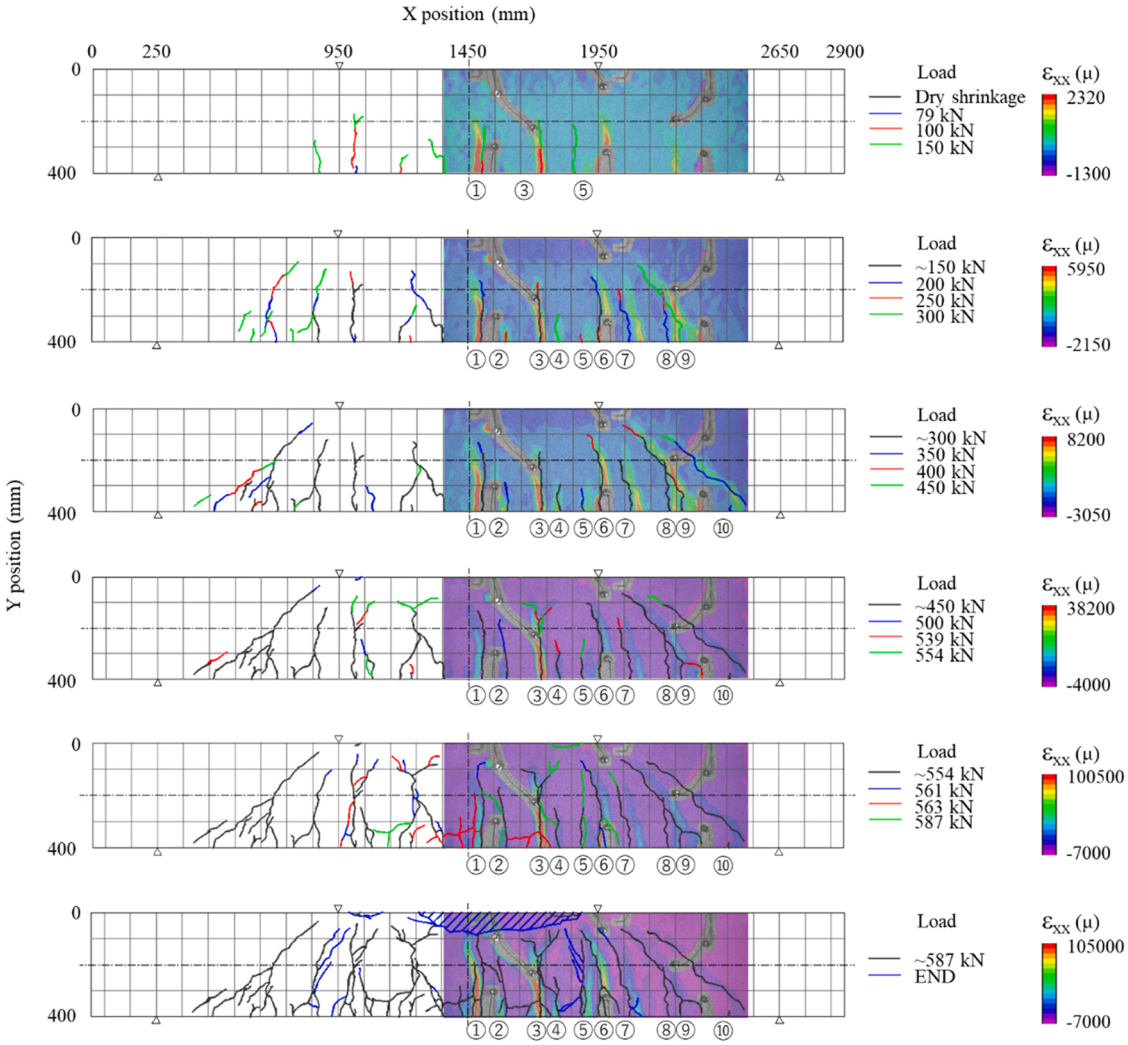

Fig. 10. Crack pattern and strain localization of case 4 (Steel).

of steel specimens, while in BFRP cases, it is highly influenced around the cracks (see Figs. 7 and 9).

In Fig. 14 (case 3), at a position of 2100 mm, the slope of deflection changes by approximately 10%. As mentioned before, this change may be due to the decrease in the shear transfer capacity. Since BFRP reinforcement has relatively low transverse strength, the contribution of dowel action is negligible [56]. In addition, the increase in crack width (Fig. 11 (case 3), crack No. 7) tends to decrease the frictional resistance among the aggregates, resulting in a more insignificant contribution of aggregate interlock [56,57].

Furthermore, from Fig. 14 (case 1), which represents the bending span of the beam, it is possible to see that the slope is not constant. This same behavior is also seen in the bending span (1250–1950 mm) of case 3. This may be due to an occurrence of uneven loading caused by the faster crack development within the bending span. However, complementary studies should be done to clarify this behavior.

3.4. Load-strain curve and neutral axis

Fig. 15 and Fig. 16 show the strain (ε_{xx}: normal strain on the cross-section directed to the X axis) of the reinforcement and concrete surface under different loads. Details of A, A', and B can be found in Fig. 2. Note that the strain measurements were made by strain gauges and DIC for the reinforcements and concrete, respectively. The measurement position was at a position of 1450 mm in cases 1 and 2 and 1950 mm in cases 3 and 4 (see Fig. 2).

As shown in Fig. 15, the strain of Concrete-A and BFRP-A at the center of the beam (1450 mm) has a similar inclination until 77 kN. However, from 77 kN, while the strain inclination of concrete tends to be the same, the strain inclination of BFRP changes. In other words, the bond-slip between concrete and BFRP reinforcement starts from around 77 kN. In addition, the amount of bond-slip tends to increase as the load rises since the strain inclination is higher at the end of the test. This increase in the bond-slip may be related to the

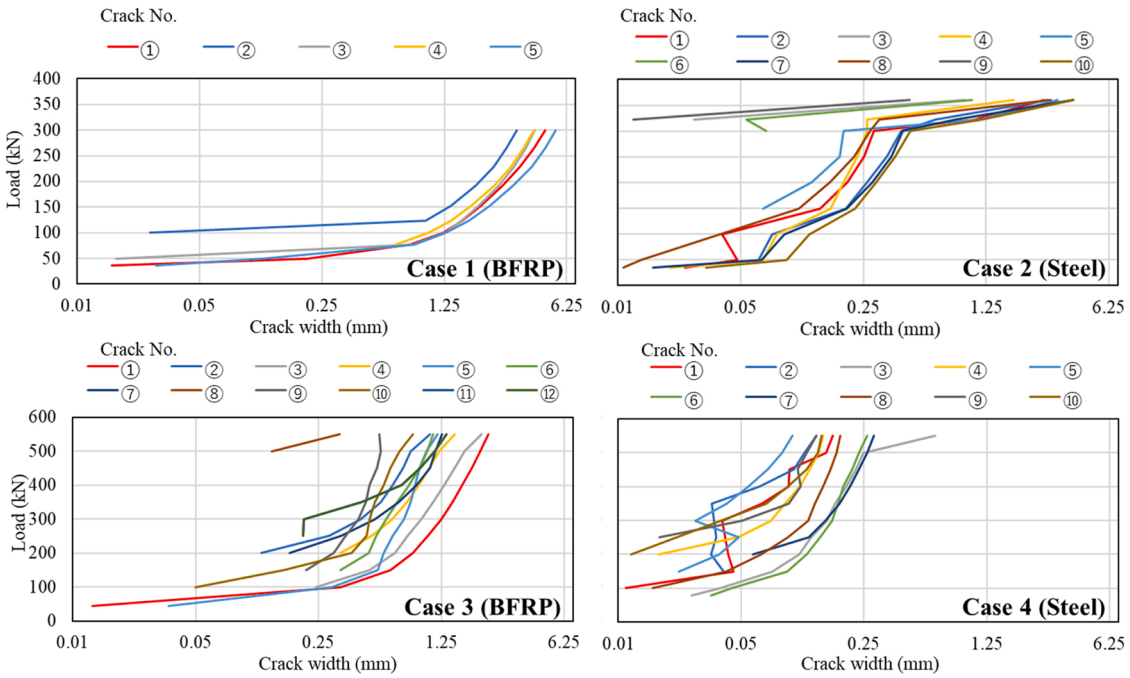

Fig. 11. Crack-width evolution during flexural loading test using DIC horizontal displacement jump at different load.

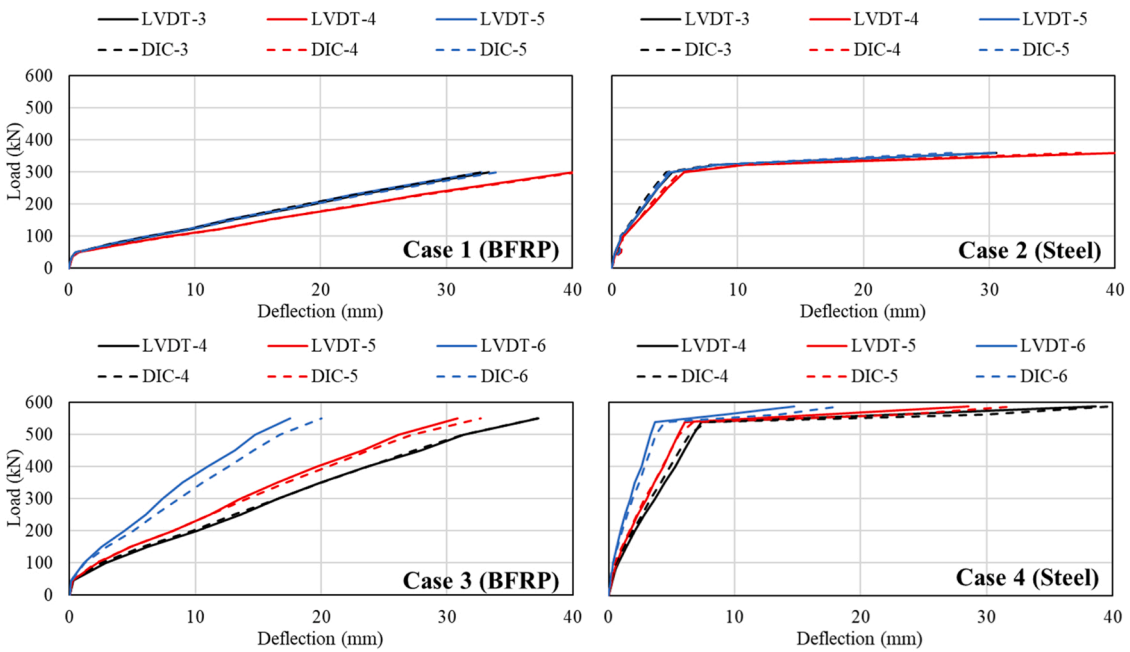

Fig. 12. Comparison of deflection obtained by LVDT and DIC.

smooth surface of BFRP bars which tends to slip easier in comparison to deformed steel bars. Furthermore, the reinforcement BFRP-B at the top of the specimen, in case 1, acts as a tensile reinforcement for practically the whole test. This may be due to the fast propagation of the cracks that reached the upper reinforcement in an early stage. On the other hand, as shown in Fig. 15, the strain inclination of Concrete-A and Steel-A at the center of the beam (1450 mm) has a similar inclination until around 322 kN.

From Fig. 16, a similar tendency of case 2 is seen in case 4. The strain inclination of Concrete-A and Steel-A is similar until around 554 kN. However, case 3 showed different behavior in comparison to case 1. The strain inclination of Concrete-A and BFRP-A and Concrete-A' and BFRP-A' changes from different load points 45 and 100 kN, respectively. Although it undulates the strain inclination

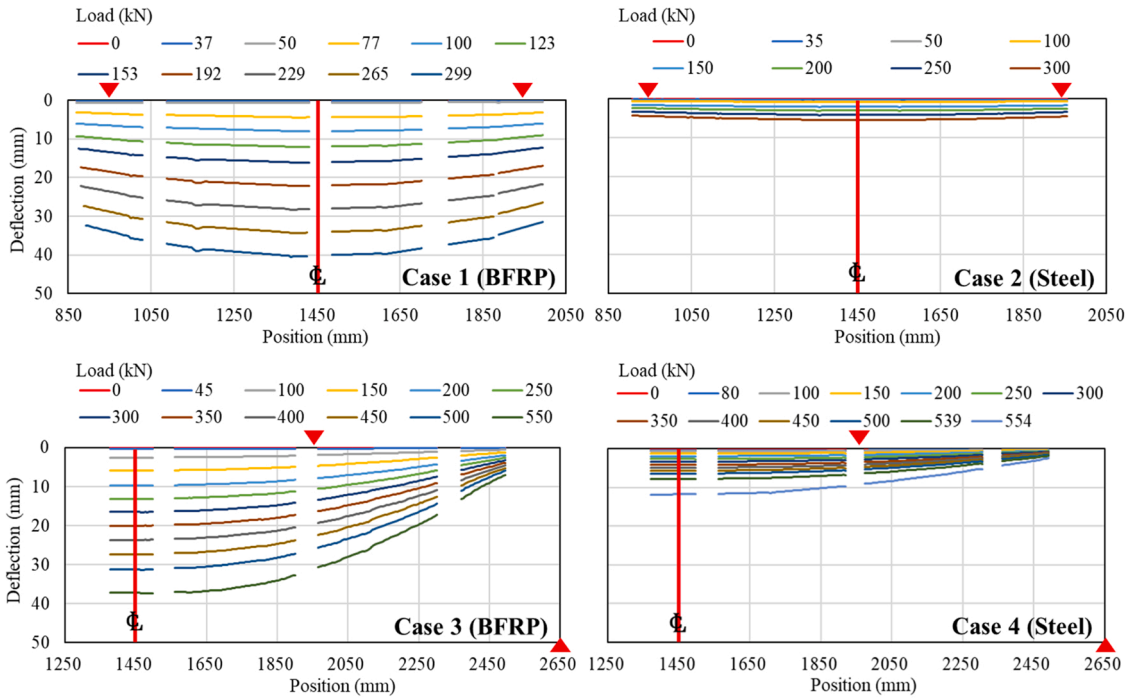

Fig. 13. Deflection of the beam subjected to different loads.

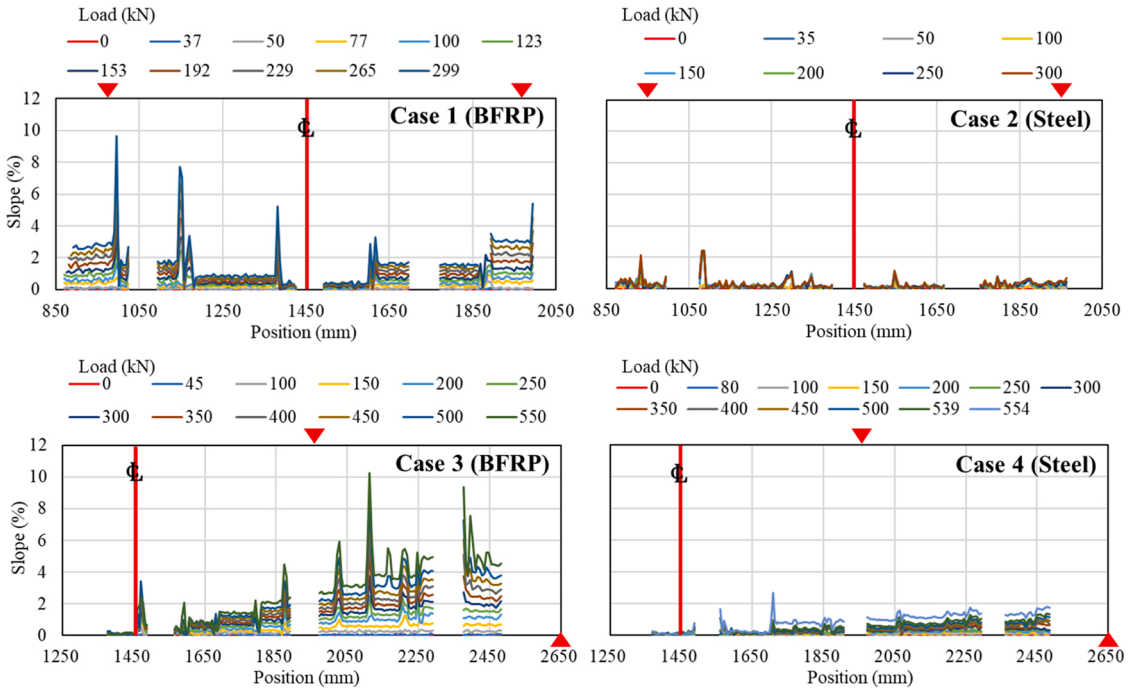

Fig. 14. Slope of deflection.

of BFRP after 100 kN, the strain inclination of both BFRP and concrete looks to be parallel until the end of the test. Unlike case 1, the bond-slip between concrete and BFRP reinforcement near the shear spam (≥1950 mm) tends to be constant until the end of the test.

Also, from Fig. 16, it is possible to see that a bond slip between Concrete-B and BFRP-B reinforcement at the top near shear spam tends to happen from 200 kN. This same behavior could also be seen in case 4. However, it starts later, around 530 kN, after the steel bars bar reaches its yield point. This is possibly due to the development of the crack at the shear spam, and the lower shear transfer

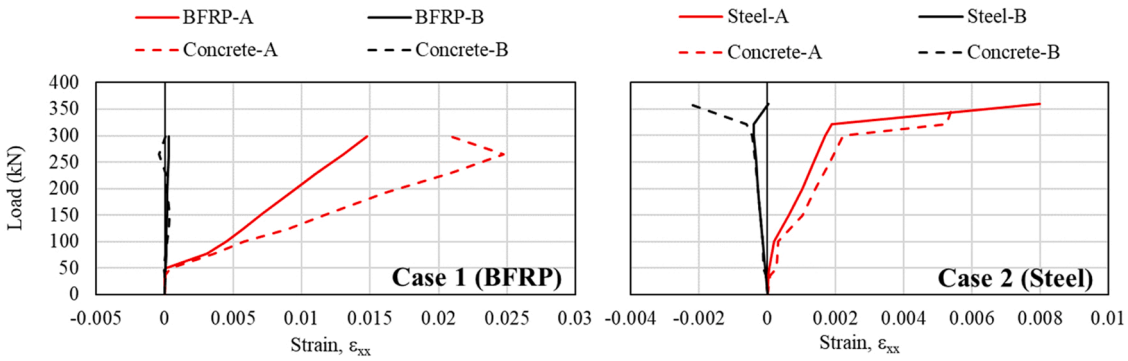

Fig. 15. Load-strain curve of cases 1 and 2 at a position of 1450 mm.

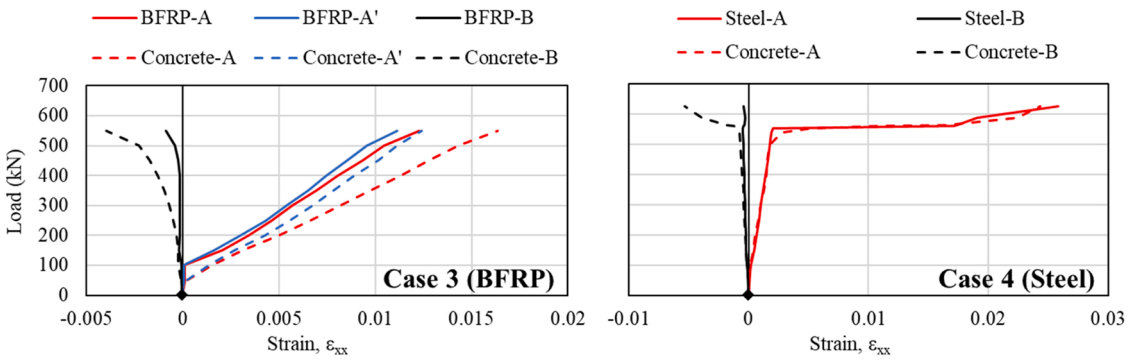

Fig. 16. Load-strain curve of cases 3 and 4 at a position of 1950 mm.

capacity of BFRP makes the compressive region of the beams be earlier influenced by the load in the case of BFRP in comparison to the steel bars case.

Fig. 17 shows the neutral axis depth during the flexural test. Note that the number of strain measurement points at the bending span was 14400 for cases 1 and 2 and 7416 for cases 3 and 4. For all cases, the distance from each other measurement point was 5 mm. By using DIC, the surface strain measurement can be done at several points, which can obtain the neutral axis accurately. As shown in Fig. 17, the neutral axis of cases 1 and 3 move upward towards the compression region of the beams and reach the value of 37.5 and 72.5 mm at 100 and 150 kN, respectively. The neutral axis depth decreases faster in BFRP cases since the cracks tend to develop in an early stage than in steel cases, as shown in Figs. 7, 8, 9, and 10. Right after the neutral axis depth decreases, the neutral axis stabilizes with the stabilization of the crack development within the bending span. On the other hand, the neutral axis in the cases of steel reinforced beams differs from BFRP cases. The neutral axis moves toward the top of the beam and stabilizes for a period in stages. This cycle repeats as the load increases and the crack development tends to increase. Although there are differences in the progress of cracks and fracture morphology, it was verified that there is no change in the feasibility of the load carrying mechanism represented by the

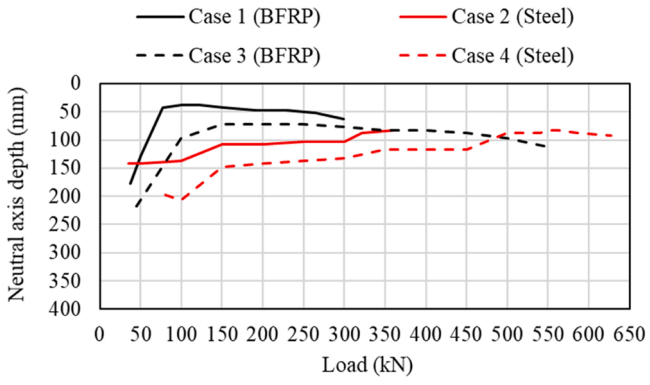

Fig. 17. Neutral axis depth at the bending span.

balance in the cross-section of bending and tension.

4. Conclusions

In this study, seven-bundled BFRP bars were applied to reinforce concrete flexural members, and the load-carrying behavior was investigated. Even small-diameter BFRP bar is bundled together to increase the diameter to ensure the designed ultimate strength, the bundled BFRP bar was consistent with the designed ultimate strength, and even though the bundled BFRP bar slightly slipped, it did not significantly affect the load carrying behavior. The main results obtained in this study can be summarized as follows.

1. Even the reinforcement used in BFRP cases was bundled bars, similar load carrying capacities were obtained in BFRP in comparison to the designed values, 364 kN for a reinforcement ratio of 0.71% and 551 kN for a reinforcement ratio of 1.66%.
2. Low BFRP reinforcement ratio exhibited a lower number of flexural and shear cracking than that case of high BFRP reinforcement ratio. In addition, the cracking spacing is larger in the low BFRP reinforcement ratio compared to the higher BFRP reinforcement ratio. On the other hand, the beams reinforced with deformed steel bars showed a larger number of cracks when compared to BFRP specimens. However, the crack width in steel cases is smaller than in BFRP cases.
3. Although the deflection is higher in BFRP cases compared to steel cases, by increasing the BFRP reinforcement ratio from 0.71% to 1.66% the deflection was reduced from 40.2 mm to 16.5 mm under a load of 300 kN, a reduction of around 59%.
4. Differences between the load-strain curves of the concrete and the reinforcement at the same depth showed that the bond-slip of BFRP cases starts earlier than in steel cases. In addition, the slip amount in the case of BFRP tends to be higher than that of the steel case.
5. While neutral axis in the cases of BFRP beams moves towards the upper end of the beam at an earlier stage, under 100 and 150 kN, for low and high reinforcement ratios, respectively, the neutral axis of steel cases reaches its maximum depths after the steel bar reaches its yield point.

Declaration of Competing Interest

The authors declare that they have no known competing financial interests or personal relationships that could have appeared to influence the work reported in this paper.

Data Availability

No data was used for the research described in the article.

Acknowledgments

This research was promoted by COI program Construction of next-generation infrastructure using innovative materials ~ Realization of a safe and secure society that can coexist with the Earth for centuries ~ supported by MEXT and JST.

References

[1] Jason Duic, Sara Kenno, Sreekanta Das, Performance of concrete beams reinforced with basalt fibre composite rebar, Constr. Build. Mater. vol. 176 (2018) 470–481.
[2] Redouan El Ghadioui, Tilo Proske, Ngoc Linh Tran, Carl-Alexander Graubner, Structural behaviour of CFRP reinforced concrete members under bending and shear loads, Mater. Struct. vol. 53 (63) (2020) 63.
[3] G. Sharma, S. Sharma, S.K. Sharma, Fracture monitoring of steel and GFRP reinforced concrete beams using acoustic emission and digital image correlation techniques, Struct. Concr. vol. 22 (2021) 1962–1976.
[4] Shamsad Ahmad, Reinforcement corrosion in concrete structures, its monitoring and service life prediction—a review, Cem. Concr. Compos. vol. 25 (4–5) (2003) 459–471.
[5] Mohamed Soliman, Dan M. Frangopol, Life-cycle cost evaluation of conventional and corrosion-resistant steel for bridges, J. Bridge Eng. vol. 20 (1) (2015).
[6] E. Sola, J. Ožbolt, G. Balabanić, Z.M. Mir, Experimental and numerical study of accelerated corrosion of steel reinforcement in concrete: transport of corrosion products, Cem. Concr. Res. vol. 120 (2019) 119–131.
[7] Jinjie Shi, Jing Ming, Wei Sun, Yamei Zhang, Corrosion performance of reinforcing steel in concrete under simultaneous flexural load and chlorides attack, Constr. Build. Mater. vol. 149 (2017) 315–326.
[8] Ueli M. Angst, Bernhard Elsener, Claus K. Larsen, Øystein Vennesland, Chloride induced reinforcement corrosion: electrochemical monitoring of initiation stage and chloride threshold values, Corros. Sci. vol. 53 (4) (2011) 1451–1464.
[9] M.F. Montemor, A.M.P. Simões, M.G.S. Ferreira, Chloride-induced corrosion on reinforcing steel: from the fundamentals to the monitoring techniques, Cem. Concr. Compos. vol. 2003 (2003) 491–502.
[10] Rita Maria Ghantous, Stéphane Poyet, Valérie L'Hostis, Nhu-Cuong Tran, Raoul François, Effect of crack openings on carbonation-induced corrosion, Cem. Concr. Res. vol. 95 (2017) 257–269.
[11] Jing Ming, Miao Wu, Jinjie Shi, Passive film modification by concrete carbonation: re-visiting a corrosion-resistant steel with Cr and Mo, Cem. Concr. Compos. vol. 123 (2021), 104178.
[12] M. Stefanoni, U. Angst, B. Elsener, Corrosion rate of carbon steel in carbonated concrete – a critical review, Cem. Concr. Res. vol. 103 (2018) 35–48.
[13] Anant Saraogi, Vilas Warudkar, Study of performance parameters of fusion bonded epoxy coated reinforcing bars and their testing, Mater. Today.: Proc. vol. 5 (2–1) (2018) 4138–4148.
[14] J.J. Chang, W. Yeih, C.L. Tsai, Enhancement of bond strength for epoxy-coated rebar using river sand, Constr. Build. Mater. vol. 16 (8) (2002) 465–472.
[15] Francisco Javier Luna Molina, María Cruz Alonso Alonso, Enrique Hernández Montes, Cecilio L.ópez Hombrados, Galvanized steel in concrete: more durable structures maintaining the bond length, J. Mater. Civ. Eng. vol. 29 (2017).

[16] E. Gudonis, E. Timinskas, V. Gribniak, G. Kaklauskas, A.K. Arnautov, V. Tamulėnas, FRP reinforcement for concrete structures: state-of-the-art review of application and design, Eng. Struct. Technol. vol. 5 (4) (2014) 147–158.
[17] S.H. Alsayed, Y.A. Al-Salloum, T.H. Almusallam, Performance of glass fiber reinforced plastic bars as a reinforcing material for concrete structures, Compos. Part B Eng. vol. 31 (6–7) (2000) 555–567.
[18] Omrani, Mohammad Hossein, Dehestani, Mehdi, Yousefpour, Hossein, Flexural behavior of lightweight concrete beams reinforced with GFRP bars and prestressed with steel strands, Struct. Concr. vol. 22 (2021) 69–80.
[19] Antonio Nanni, North American design guidelines for concrete reinforcement and strengthening using FRP: principles, applications and unresolved issues, Constr. Build. Mater. vol. 17 (6–7) (2003) 439–446.
[20] Toyo Miyagawa, Maki Yoshida, Atsushi Hattori, Kaoru Iwamoto, Alkali resistance of fiber reinforced plastic for use in concrete structures, Concr. Libr. Int. vol. 27 (1996) 177–188.
[21] Martin Alberto Masuelli, Fiber Reinforced Polymers - The Technology Applied for Concrete Repair, Rijeka: IntechOpen, 2013.
[22] Muhammad Masood Rafi, Ali Nadjai, Experimental behaviour of carbon FRP reinforced concrete beams at ambient and elevated temperatures, J. Adv. Concr. Technol. vol. 6 (2008) 431–441.
[23] Mohamed Saafi, Houssam Toutanji, Flexural capacity of prestressed concrete beams reinforced with aramid fiber reinforced polymer (AFRP) rectangular tendons, Constr. Build. Mater. vol. 12 (5) (1998) 245–249.
[24] G. Karayannis, Chris, K. Kosmidou, Parthena-Maria, E. Chalioris, Constantin, Reinforced concrete beams with carbon-fiber-reinforced polymer bars—experimental study, Fibers vol. 6 (4) (2018) 99.
[25] Charles E. Bakis, Thomas E. Boothby, Junhui Jia, Bond durability of glass fiber-reinforced polymer bars embedded in concrete beams, J. Compos. Constr. vol. 11 (3) (2007) 269–278.
[26] Yi Chen, Julio F. Davalos, Indrajit Ray, Hyeong-Yeol Kim, Accelerated aging tests for evaluations of durability performance of FRP reinforcing bars for concrete structures, Compos. Struct. vol. 78 (1) (2007) 101–111.
[27] N.F. Grace, A.K. Soliman, G. Abdel-Sayed, K.R. Saleh, Behavior and ductility of simple and continuous FRP reinforced beams, J. Compos. Constr. vol. 2 (2) (1998) 186–194.
[28] Yu Zheng, Lingzhu Zhou, Su.E. Taylor, Hongwei Ma, Serviceability of one-way high-volume fly ash-self-compacting concrete slabs reinforced with basalt FRP bars, Constr. Build. Mater. vol. 217 (2019) 108–127.
[29] Andreea Serbescu, Maurizio Guadagnini, Kypros Pilakoutas, Mechanical characterization of basalt FRP rebars and long-term strength predictive model, J. Compos. Constr. vol. 19 (2) (2015).
[30] Douglas Tomlinson, Amir Fam, Performance of concrete beams reinforced with basalt FRP for flexure and shear, J. Compos. Constr. vol. 19 (2) (2015).
[31] Fareed Elgabbas, Ehab A. Ahmed, Brahim Benmokrane, Physical and mechanical characteristics of new basalt-FRP bars for reinforcing concrete structures, Constr. Build. Mater. vol. 95 (2015) 623–635.
[32] Swapnasarit Kar, K.C. Biswal, External shear strengthening of RC beams with basalt fiber sheets: an experimental study, Structures vol. 31 (2021) 305–315.
[33] Weidong He, Xin Wang, Lining Ding, Zhishen Wu, Efficiency of different BFRP-based strengthening techniques in improving flexural behavior of RC slabs, Constr. Build. Mater. vol. 308 (2021), 125002.
[34] Vivek Dhand, Garima Mittal, Kyong Yop Rhee, Soo-Jin Park, David Hui, A short review on basalt fiber reinforced polymer composites, Compos. Part B Eng. vol. 73 (2015) 166–180.
[35] B. Sagar, M.V.N. Sivakumar, Performance evaluation of basalt fibre-reinforced polymer rebars in structural concrete members–a review, Innov. Infrastruct. Solut. vol. 6 (75) (2021) 75.
[36] JIS A 5308, Ready-mixed concrete, 2019.
[37] JIS A 1108, Method of test for compressive strength of concrete, 2018.
[38] JIS A 1149, Method of test for static modulus of elasticity of concrete, 2017.
[39] JIS A 1101, Method of test for slump of concrete, 2020.
[40] JIS G 3112, Steel bars for concrete reinforcement, 2020.
[41] Japan Society of Civil Engineers, Design and construction guidelines for concrete structures using continuous fiber reinforcement -draft-, Concrete Library 88, 1996.
[42] JIS A 1106, Method of test for flexural strength of concrete, 2018.
[43] David Corr, Matteo Accardi, Lori Graham-Brady, Surendra Shah, Digital image correlation analysis of interfacial debonding properties and fracture behavior in concrete, Eng. Fract. Mech. vol. 74 (1) (2007) 109–121.
[44] S.G. Shah, J.M. Chandra Kishen, Fracture properties of concrete–concrete interfaces using digital image correlation, Exp. Mech. vol. 51 (2011) 303–313.
[45] Tahreer M. Fayyad, Janet M. Lees, Application of digital image correlation to reinforced concrete fracture, Procedia Mater. Sci. vol. 3 (2014) 1585–1590.
[46] B. Omondi, D.G. Aggelis, H. Sol, C. Sitters, Improved crack monitoring in structural concrete by combined acoustic emission and digital image correlation techniques, Struct. Health Monit. vol. 15 (3) (2016) 359–378.
[47] Wenjie Ge, Jiwen Zhang, Dafu Cao, Yongming Tu, Flexural behaviors of hybrid concrete beams reinforced with BFRP bars and steel bars, Constr. Build. Mater. vol. 87 (2015) 28–37.
[48] Farid Abed, Abdul Rahman Alhafiz, Effect of basalt fibers on the flexural behavior of concrete beams reinforced with BFRP bars, Compos. Struct. vol. 2015 (2019) 23–34.
[49] Fareed Elgabbas, Patrick Vincent, Ehab A. Ahmed, Brahim Benmokrane, Experimental testing of basalt-fiber-reinforced polymer bars in concrete beams, Compos. Part B Eng. vol. 91 (2016) 205–218.
[50] Ahmed El Refai, Farid Abed, Abdullah Al-Rahmani, Structural performance and serviceability of concrete beams reinforced with hybrid (GFRP and steel) bars, Constr. Build. Mater. vol. 96 (2015) 518–529.
[51] Fareed Elgabbas, Ehab A. Ahmed, M. ASCE, Brahim Benmokrane, Flexural behavior of concrete beams reinforced with ribbed basalt-FRP bars under static loads, J. Compos. Constr. vol. 21 (3) (2016).
[52] J.F. Destrebecq, E. Toussaint, E. Ferrier, Analysis of cracks and deformations in a full scale reinforced concrete beam using a digital image correlation technique, Exp. Mech. vol. 51 (2011) 879–890.
[53] Mohamed F.M. Fahmy, ShehabEldeen A.S. Ahmed, Zhishen Wu, Bar surface treatment effect on the bond-slip behavior and mechanism of basalt FRP bars embedded in concrete, Constr. Build. Mater. vol. 289 (2021), 122844.
[54] Sandor Solyom, György L. Balázs, Bond of FRP bars with different surface characteristics, Constr. Build. Mater. vol. 264 (2020), 119839.
[55] Xiaoshan Lin, Y.X. Zhang, Bond–slip behaviour of FRP-reinforced concrete beams, Constr. Build. Mater. vol. 44 (2013) 110–117.
[56] Mohsen A. Issa, Thilan Ovitigala, Mustapha Ibrahim, Shear behavior of basalt fiber reinforced concrete beams with and without basalt FRP stirrups, J. Compos. Constr. vol. 20 (4) (2016).
[57] A. Tureyen, R.J. Frosch, Shear tests of FRP-reinforced concrete beams without stirrups, Acids Struct. J. vol. 99 (4) (2002) 427–434.